symmetry

MDPI

Article

Negative Solvatochromism of the Intramolecular Charge Transfer Band in Two Structurally Related Pyridazinium—Ylids

Mihaela Iuliana Avădănei [1,*], Antonina Grițco-Todirașcu [2] and Dana Ortansa Dorohoi [3,*]

[1] "Petru Poni" Institute of Macromolecular Chemistry, 41A Gr. Ghica Voda Alley, 700487 Iasi, Romania
[2] "Ion Creanga" Gymnazial School, 119 Toma Cozma Street, 700312 Iasi, Romania; antoninagritco@yahoo.com
[3] Faculty of Physics, "Alexandru Ioan Cuza" University, 11 Carol Blvd, 700454 Iasi, Romania
* Correspondence: mavadanei@icmpp.ro (M.I.A.); ddorohoi@uaic.ro (D.O.D.)

Abstract: Two charge transfer compounds based on pyridazinium ylids were studied by electronic absorption spectroscopy in binary and ternary solutions, with the purpose of evaluating their descriptors of the first singlet excited state and to estimate the strength of the intermolecular interactions in protic solvents. The molecular descriptors of the excited state were comparatively estimated using the variational method and the Abe model of diluted binary solutions. Analysis of electronic properties using density functional theory was performed for several key solvents, in order to understand the solvatochromic behavior. The DFT calculations revealed that, in the polar and strongly interacting solvents, the carbanion and the terminal group become a stronger electron acceptor. The bathochromic shift of the ICT band was confirmed using DFT calculus. The ability of the two ylids to recognize and discriminate the solvents was analyzed with principal component analysis and with cluster analysis. Although the study was performed in 24 solvents, the results showed that the ylids were most sensitive to alcohols, so they can be a useful tool to identify and classify different types of low-alcoholic solvents.

Keywords: pyridazinium ylids; intramolecular charge transfer visible band; ternary solutions; molecular orbitals; solvatochromism; Abe model

Citation: Avădănei, M.I.; Grițco-Todirașcu, A.; Dorohoi, D.O. Negative Solvatochromism of the Intramolecular Charge Transfer Band in Two Structurally Related Pyridazinium—Ylids. *Symmetry* **2024**, *16*, 1531. https://doi.org/10.3390/sym16111531

Academic Editor: György Keglevich

Received: 2 October 2024
Revised: 4 November 2024
Accepted: 8 November 2024
Published: 15 November 2024

1. Introduction

Pyridazinium ylids belong to the cycloimmonium class [1,2] and because of their dipolar nature play an important role in the synthesis of heterocyclic compounds, and they can be used as acid–base indicators, analytical reagents for obtaining medicines in situ, and as biological agents [3–7], as anticancer [8,9], antituberculosis [10], or antimicrobial [11] compounds. Ylids have a zwitterionic structure, where the positively charged nitrogen atom of the pyridazinium ring is covalently bonded to a negative-charged carbanion. The ylids are highly polar molecules with dipolar moments, whose stability increases with the electronegativity of the substituents at the carbanion. In general, disubstituted cycloimmonium ylids are more stable than monosubstituted ylids, but the latter type is easily utilized in the chemical reactions or dimerizations [2,3] used to obtain the heterocycles applied in pharmaceutics industry [4–12]. As precursors for obtaining special kinds of medicines, knowledge about their intermolecular interactions in solutions becomes an important topic.

The study presented in this manuscript concerns two mono-substituted *p*-phenacyl pyridazinium ylids, namely *p*-phenyl-*p*′-phenyl-pyridazinium-*p*-nitro-phenacylid (PPPyNiP) and pyridazinium-*p*-nitro-phenacylid (PyNiP). Their chemical structure is presented in Figure 1. A preliminary spectral and computational study revealed their relative stability and basic character [12]. The electronegative fragment *p*-nitro-phenacyl gives a relative stability to the molecule by increasing the negative charge delocalization on the carbanion. In the visible absorption process, the negative charge is shifted from the carbanion to the

phenacyl group, in a direction that is in opposition with that commonly observed in other cycloimmonium ylids (such as pyridinium or iso-quinolinium ylids [1,13]).

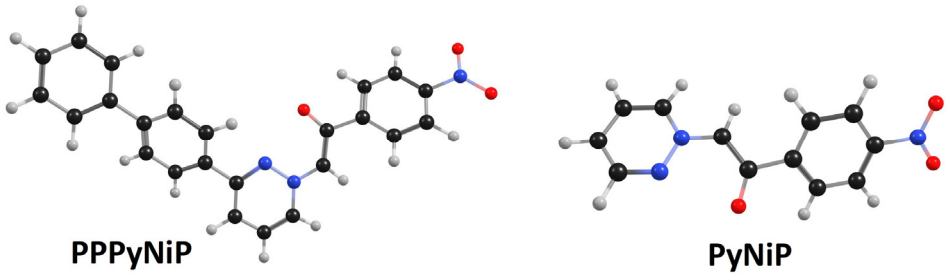

Figure 1. Energy minimized structures in the ground state of PPPyNiP and PyNiP in vacuo and with the corresponding atomic charges. Level of theory: DFT-ω-B97X-D/STO-3G/def2SV (carbon black; hydrogen grey; nitrogen blue; oxygen red).

The charge separation on the ylid bond $N^+ - C^-$ provides the basic character in the ground state of the studied molecules, which determines their ability to participate in intermolecular hydrogen bonding with the hydroxyl group of alcohols or carboxylic acids. These intermolecular interactions are facilitated by the carbanion in the *sp*3 hybridization, the presence of a pair of non-participating electrons on the carbanion, and the high electronegativity of the nitro group belonging to the carbanion substituent. These specific interactions in solution can be spectrally observed by the blue shift of the charge transfer band (ICT) in the electronic absorption spectra. Previous studies provided evidence of the prevalence of universal interactions in the binary solutions of some pyridazinium ylids [14–16], which are supplemented by specific interactions in hydroxylic solvents, especially manifested by accepting protons from the solvent. This conclusion gains support from the dependence of the maximum of the ICT band on the solvent parameters [14–16].

Our study focused on evaluation of the molecular descriptors in the excited state, which was performed through a comparative approach, employing two methods: the variational method [17] and the Abe model [18]. In the second part, a spectral analysis of ternary solutions of PPPyNiP and PyNiP based on the statistic cell model [19,20] was carried out, with the purpose of estimating the strength of the specific interactions in protic solvents. DFT and TD-DFT calculations were employed to determine certain electronic properties in the ground and the excited state, and to analyze the frontier and the natural transition orbitals. The final part of our study considered the solvatochromism of the ICT band as a sensing element for recognition and discrimination of solvents based on their coordinating properties.

2. Materials and Methods

The synthesis and structural characterization of PPPyNiP and PyNiP have previously been described [1,12]. The electronic absorption spectra were recorded with an Analytic Jena Specord Plus-5 spectrophotometer, in quartz cuvettes of 10 mm pathlength. All solvents were of spectral grade, acquired from Chemopar® (Iasi, Romania), Sigma-Aldrich ® and Merck® (St. Louis, MO, USA). When required, the solvent was purified [21,22]. The Kamlet–Taft microscopic (α and β) and macroscopic parameters (f(ε) and f(*n*)) were obtained from previous studies [12,23–27] and are listed in Table 1. The wavenumbers of the maximum of the ICT band are also listed in Table 1.

Table 1. The Kamlet–Taft solvent parameters and the wavenumber in the maximum of the ICT band of PPPyNiP and PyNiP.

	Solvent	**f(ε)**	**f(n)**	β	α	π^*	$\nu\ (\mathbf{cm^{-1}})$ **PPPyNiP**	$\nu\ (\mathbf{cm^{-1}})$ **PyNiP**
1	Cyclohexane	0.254	0.256	0.00	0.00	0	19,700	19,900
2	Toluene	0.315	0.293	0.11	0.00	0.49	19,900	20,100
3	Anisole	0.524	0.303	0.32	0.00	0.73	20,100	20,170
4	Diethyl ether	0.526	0.217	0.47	0.00	0.24	20,100	20,300
5	Chloroform	0.559	0.267	0.10	0.20	0.53	20,550	20,720
6	Butyl acetate	0.576	0.239	0.45	0.00	0.46	20,330	20,440
7	Ethyl acetate	0.626	0.227	0.45	0.10	0.55	20,450	20,660
8	Pyridine	0.652	0.299	0.52	0.00	0.9	20,250	20,270
9	Tetrahydrofuran	0.687	0.246	0.55	0.00	0.55	20,150	20,340
11	1,2Dichloroethane	0.757	0.266	0.10	0.00	0.48	20,600	20,830
10	1-Pentanol	0.811	0.247	0.86	0.84	0.15	21,000	21,180
12	Iso-Butanol	0.845	o.240	0.84	0.79	0.15	21,150	21,250
13	1-Butanol	0.849	0.242	0.93	0.42	0.47	21,100	21,320
14	2-Propanol	0.849	0.230	0.84	0.76	0.48	21,160	21,250
15	Acetophenone	0.850	0.311	0.49	0.04	0.81	20,750	20,700
16	1-Propanol	0.864	0.235	0.90	0.84	0.52	21,200	21,360
17	Acetone	0.864	0.219	0.48	0.08	0.62	20,700	20,830
18	Ethanol	0.887	0.221	0.75	0.86	0.54	21,350	21,410
19	Acetonitril	0.913	0.212	0.40	0.19	0.66	20,850	20,940
20	Methanol	0.914	0.203	0.66	0.98	0.6	21,460	21,640
21	DMF	0.922	0.259	0.69	0.00	0.88	20,530	20,700
22	DMSO	0.938	0.283	0.76	0.00	1	20,600	20,700
23	Water	0.964	0.204	0.50	1.20	1.2	21,650	21,860
24	Formamide	0.982	0.267	0.48	0.71	0.97	20,410	21,200

The binary solvents were achieved in volumetric percentages C_1 and C_2, with $C_1 + C_2 = 1$. Then, the molar concentrations x_1 and x_2 were computed using the following expressions:

$$x_1 = \frac{C_1 \frac{\rho_1}{M_1}}{C_1 \frac{\rho_1}{M_1} + C_2 \frac{\rho_2}{M_2}} \quad \text{and} \quad x_2 = 1 - x_1 \tag{1}$$

The index '1' marks the solvent with the strongest interacting abilities. The density, ρ, and the molar mass of the two solvents are known.

Computational details. The electronic structure of the compounds was analyzed using the Gaussian 09W A.01 software [28]. The relaxed geometries were calculated in vacuo without symmetry constraints, while the effect of the solvent was addressed in the polarizable continuum model (IEF-PCM) for cyclohexane, methanol, and dimethylsulfoxide. The minimum on the potential energy surface in every case was verified by calculating the harmonical vibrational frequencies. Density functional theory (DFT) and time-dependent TD-DFT were used with the range-separated functional ω-B97X-D and the STO-3G/def2SV basis set, taking into account the reported effects of electron correlation and long-range correction on the optical properties [29]. The natural transition orbitals (NTO) were calculated using the same methodology.

Statistical analysis. The spectral data were analyzed by principal component analysis and cluster analysis using Orange 3.33^{TM} software.

3. Results and Discussion

3.1. Spectral Study in Binary Solutions

The structures of PPPyNiP and PyNiP are presented in Figure 1 as calculated optimized geometries in vacuo, at the ω-B97X-D/STO-3G/def2SV level of theory. In a previous study, we obtained their electronic absorption spectra in a series of solvents, with polarity and coordinating ability of various types, and ranging from non-polar to very polar alcohols (Table 1). We observed that the ylids showed an intense π-π* absorption band in the UV region, which had a low sensitivity to the solvent's type, and a weak Vis band attributed to an intramolecular charge transfer (ICT) between the heterocycle and the carbanion [12–16,30]. The ICT band was very sensitive to the nature of the solvent, shifting to the blue in hydroxylic solvents (alcohols and carboxylic acids) and to the red in nonpolar solvents (Table 1).

The solvatochromic behavior of PPPyNiP and PyNiP was analyzed by applying Equation (2) [31–33] that links the maximum of the ICT band to the parameters of the solvent:

$$\nu_{comp.}\left(\mathrm{cm}^{-1}\right) = \nu_0 + C_1 f(\varepsilon) + C_2 f(n) + C_3\beta + C_4\alpha \quad (2)$$

We extended the previously reported study [12] with a series of new experimental data, and Table 1 gathers the whole set of ICT band values. In Equation (2), the free term ν_0 signifies the wavenumber in gaseous phase; the two following terms describe the universal interactions of the orientation, induction, polarization, and dispersion types that are dependent on the dielectric permittivity, ε, and the refractive index of the solvent, n. The last two terms in Equation (2) give the influence of specific interactions on the position of the ICT band. The microscopic parameters β and α describe the ability of the solvent to accept or to donate a proton when hydrogen bonding with the solute occurs.

The C_1–C_4 coefficients in Equation (2) were calculated by multiple linear regression and the results are presented in Table 2.

Table 2. Multiple linear regression performed on Equation (2) for PPPyNiP and PyNiP.

		$\mathbf{R^2}$
PPPyNiP	$\nu\left(\mathrm{cm}^{-1}\right) = 20,117 + 1076{\cdot}f(\varepsilon) - 2046{\cdot}f(n) - 90.50{\cdot}\beta + 624.8{\cdot}\alpha$	0.84
PyNiP	$\nu\left(\mathrm{cm}^{-1}\right) = 20,191 + 1254{\cdot}f(\varepsilon) - 1847{\cdot}f(n) - 158.4{\cdot}\beta + 759.8{\cdot}\alpha$	0.94

By using the coefficients expressing the contribution of universal interactions to the ICT wavenumbers, the excited state dipole moments of the two ylids can be calculated. The following relations are used:

$$C_1 = \frac{2\mu_g\left(\mu_g - \mu_e cos\varphi\right)}{r^3} + 3KT\frac{\alpha_g - \alpha_e}{r^3} \quad (3)$$

$$C_2 = \frac{\mu_g^2 - \mu_e^2}{r^3} - \frac{2\mu_g\left(\mu_g - \mu_e cos\varphi\right)}{r^3} - 3KT\frac{\alpha_g - \alpha_e}{r^3} + \frac{3}{2}\frac{I_u I_v}{I_u + I_v}\frac{\alpha_g - \alpha_e}{r^3} \quad (4)$$

The notations μ, α, I, and r signify the electric dipole moment, the electric polarizability, the ionic potential, and the molecular radius of the molecule, respectively. The indices g and e stand for the ground and excited state of the solute, respectively. Notations u and v correspond to the solute and the solvent molecule. The coefficients C_1 and C_2 from Equations (3) and (4) were determined by statistical methods using the data in Table 1, and they are listed in Table 2. The ground state descriptors of PPPyNiP and PyNiP and the ionization potentials were previously calculated [12].

Equations (3) and (4) contain three unknown parameters: μ_e, α_e, and the angle φ between the dipole moments in the electronic states responsible for the appearance of the ICT band. Because the two equations contain three unknown parameters, the variational method can be applied in order to estimate, within the limits of the approximation in which the liquid theories are developed, the excited state dipole moment of the solute. One can use the theory of McRae, which states that the electric polarizability of the solute does not change from the ground to the excited state [34,35]. The solute parameters in the ground state of PPPyNiP and PyNiP were previously calculated using HyperChem® and were reported in [12].

The increase in the dipole moment in the excited state relative to the ground state occurs in the direction of the charge transition from the carbanion towards the phenacyl substituent, whose -NO_2 substituent bears a high electronegativity. The shift to blue of the ICT band in hydroxylic solvents is due to the increase in the ground state dipole moment, because hydrogen bonds are established between the carbanion of the ylid and the -OH group of the solvent.

From the data in Tables 3 and 4, it can be seen that the estimated excited state dipole moment of both ylids is higher than in the ground state. This result is acceptable when we take into account that the charge transfer takes place from the heterocycle to the *p*-nitro-phenacyl substituent in both PPPyNiP and PyNiP, which is in opposition to what occurs in carbanion disubstituted pyridinium ylids [1,13] or in carbanion disubstituted iso-quinolinium ylids [36,37]. Additionally, the empirical McRae hypothesis regarding the conservation of the electric permittivity of the ylids during the absorption process can induce variations in the calculated values of μ_e.

Table 3. The excited state dipole moments and the angle φ between the dipole moments estimated by the variational method when the molecular descriptors are calculated using DFT for one isolated molecule [12].

Molecule		**Parameters**
PPPyNiP	$\alpha_e = 52.2153 - 0.0856\mu_e^2$ $0.0104 - 16.88\ \mu_e cos\varphi + 112.1744 = 0$ $C_1 = 1076\ cm^{-1}$; $C_2 = -2046\ cm^{-1}$; $E_{HOMO} = -8.71\ eV$; $I_{CHX} = 11\ eV$	$\mu_e = 9.89D$; φ = 47.3°; $\alpha_e = 43.84A^3$; $\mu_g = 8.44D$; r = 5.1526A
PyNiP	$\alpha_e = 31.1732 - 0.0869\mu_e^2$ $0.0105 - 15.88\ \mu_e cos\varphi + 96.9632 = 0$ $C_1 = 1254\ cm^{-1}$; $C_2 = -1847\ cm^{-1}$; $E_{HOMO} = -8.48\ eV$; $I_{CHX} = 11\ eV$	$\mu_e = 8.74D$; φ = 42.5°; $\alpha_e = 24.54A^3$; $\mu_g = 7.94D$; r = 4.8407A

Table 4. The excited state dipole moments and the angle φ between the dipole moments estimated by the variational method when the molecular descriptors are calculated using DFT for one molecule in cyclohexane (CHX).

Molecule		**Parameters**
PPPyNiP	$\alpha_e = 71.3572 - 0.0856\mu_e^2$ $0.0104 - 21.64\ \mu_e cos\varphi + 217.1872 = 0$ $C_1 = 1076\ cm^{-1}$; $C_2 = -2046\ cm^{-1}$; $E_{HOMO} = -7.30\ eV$; $I_{CHX} = 11\ eV$	$\mu_e = 11.98D$; φ = 32.5°; $\alpha_e = 59.07A^3$; $\mu_g = 10.82D$; $\alpha_g = 59.08A^3$; r = 5.1526A
PyNiP	$\alpha_e = 39.6532 - 0.0869\mu_e^2$ $0.0105 - 19.40\ \mu_e cos\varphi + 168.4221 = 0$ $C_1 = 1254\ cm^{-1}$; $C_2 = -1847\ cm^{-1}$; $E_{HOMO} = -7.61\ eV$; $I_{CHX} = 11\ eV$	$\mu_e = 10.14D$; φ = 30.5°; $\alpha_e = 30.72A^3$; $\mu_g = 9.70D$; $\alpha_g = 30.71A^3$; r = 4.8407A

The above relations between the correlation coefficients obtained in the solvatochromic study and the molecular descriptors of the ground state of the solute are widely used to estimate the dipole moment in the excited state. Therefore, a large number of differences between results have been reported in literature [38–45]. These discrepancies can be

induced by the simplifying hypotheses that describe the intermolecular interactions of solute–solvent or by the calculations of the molecular descriptors in the ground state of the isolated molecule, which are further drastically modified in the solvation process. Regarding the excited state of the solute, differences in the molecular descriptors can be due to the calculation method used, as forces of different nature and strength can act in each solvent [46,47].

The values of the excited state dipole moment obtained above by the variational method for PPPyNiP and PyNiP can be compared with the values obtained when the model proposed by T. Abe was applied to the same data. This model was developed for diluted binary solutions of spectrally active solute with the absorption band in the visible region [18]. As most solvents do not absorb in this part of the spectrum, analyzing the solvatochromism of a solute in a large number of solvents allows a statistical analysis of the results. The T. Abe model establishes a linear dependence between the solute parameters A and B calculated according to the following equations [18]:

$$A = \frac{\mu_g^2(v) + \frac{3}{2}\alpha_g(v)\frac{I_g(v)\left[I_g(u)-hc\nu_s\right]}{I_g(v)+I_g(u)-hc\nu_s}}{\frac{2}{3kT}\mu_g^2(v(p)) + \alpha(v)}, \tag{5}$$

$$B = \frac{\frac{\nu_0-\nu_s}{C} + \left\{\mu_g^2(v) + \frac{3}{2}\alpha_g(v)\frac{I_g(v)\left[I_g(u)-hc\nu_s\right]}{I_g(v)+I_g(u)-hc\nu_s}\right\}\alpha_g(u)}{\frac{2}{3kT}\mu_g^2(v(p)) + \alpha(v)}, \tag{6}$$

$$\mu_e^2(u) - \mu_g^2(u) + \alpha_e(u)A = B. \tag{7}$$

The constant C from relation (6) can be determined as follows [18]:

$$C = \sum_p R_{uv(p)}^{-6}$$

$$C = \frac{16\pi^3 N_A^2}{9}\left(\frac{\rho_v}{M_v}\right)^{\frac{2}{3}}\left\{\left[\left(\frac{M_u}{\rho_u}\right)^{\frac{1}{3}} + \left(\frac{M_v}{\rho_v}\right)^{\frac{1}{3}}\right]^{-4} + \left[\left(\frac{M_u}{\rho_u}\right)^{\frac{1}{3}} + 3\left(\frac{M_v}{\rho_v}\right)^{\frac{1}{3}}\right]^{-4} + \left[\left(\frac{M_u}{\rho_u}\right)^{\frac{1}{3}} + 5\left(\frac{M_v}{\rho_v}\right)^{\frac{1}{3}}\right]^{-4} + \ldots\right\} \tag{8}$$

In Equations (5)–(8), the following notations are used: μ—the electric dipole moment; α—the molecular polarizability; *I*—ionization potential; ν—wavenumber in the maximum of the electronic absorption band; *M*—molar mass; ρ—density; *T*—absolute temperature; indices *u* and *v* refer to the spectrally active molecule and to the solvent molecule, respectively; indices *g* and *e* refer to the ground and the excited states of the solute molecule; N_A—the Avogadro number; *k*—the Boltzmann constant.

In dependence B vs. A from Equation (7), the slope $\alpha_e(u)$ indicates the polarizability in the excited state of the solute molecule. The intercept has the form of $\mu_e^2(u) - \mu_g^2(u)$; therefore, it is the difference between the squares of the dipole moments in the ground and excited states of the solute, responsible for the light absorption process [48,49]. The A and B parameters from Equations (5) and (6) were calculated using the spectral data from Table 1 and with the solvent parameters from Table S1. Table 5 lists the values for both PPPyNiP and PyNiP.

A graphical representation of B as a function of A is illustrated in Figure 2. The slope and the intercept were used to determine the descriptors of the excited state (the dipole moment and the polarizability) of PPPyNiP and PyNiP. The corresponding ground state values were calculated using DFT in cyclohexane as an example, and Table 6 lists the values of these descriptors.

Table 5. The Abe parameters A and B for the visible band of PPPyNiP and PyNiP.

Nr	Solvent	PPPyNiP		PyNiP	
		$10^{12}A$	$10^{36}B$	$10^{12}A$	$10^{36}B$
1	Cyclohexane	9.596	533.118	9.344	311.606
2	Toluene	7.353	346.860	7.168	173.959
3	Anisole	2.545	120.023	2.490	52.955
4	Diethyl ether	2.655	58.988	2.314	30.535
5	Chloroform	2.687	28.016	2.616	−1.016
6	Butyl acetate	1.830	32.928	1.786	10.328
7	Ethyl acetate	1.760	59.809	1.457	0.710
8	Pyridine	0.321	−9.541	0.315	−2.490
9	Tetrahydrofuran	1.420	64.211	1.272	27.539
10	1,2 Dichloroethane	1.958	11.047	1.906	3.296
11	1-Pentanol	1.858	−31.439	1.810	−24.189
12	1-Butanol	1.535	−52.319	1.500	−41.625
13	Iso-Butanol	1.430	−121.418	1.394	−33.127
14	2-Propanol	1.392	−129.195	1.357	−46.113
15	Acetophenone	0.575	3.736	0.559	2.228
16	1-Propanol	1.215	−45.481	1.184	−39.777
17	Acetone	0.479	3.595	0.470	−0.239
18	Ethanol	0.958	−42.688	0.935	−31.300
19	Acetonitril	0.223	0.068	1.652	−0.757
20	Methanol	0.646	−14.211	0.630	−25.944
21	DMF	2.613	34.525	2.559	10.038
22	DMSO	1.431	−17.473	2.401	13.828
23	Water	0.307	−11.486	0.305	−9.507
24	Formamide	0.219	−1.464	0.216	−0.283

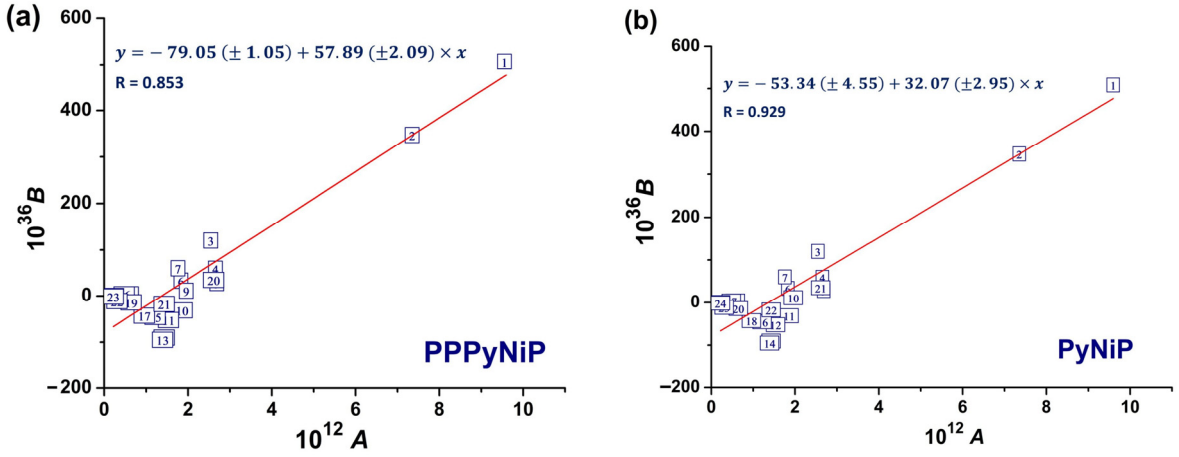

Figure 2. Plot of the Abe parameters B vs. A for (**a**) PPPyNiP and (**b**) PPNiP. The numbers correspond to the current numbering of the solvents listed in Table 5.

Table 6. The molecular parameters of PPPyNiP and PyNiP in cyclohexane, obtained using DFT calculations for the ground state, and the parameters estimated through the Abe model for the excited state.

Ylid	$\mu_g(D)$	$\alpha_g(A^3)$	$\mu_e(D)$	$\alpha_e(A^3)$
PPPyNiP	10.76	59.08	6.13	57.89
PyNiP	8.65	30.71	6.39	32.07

From Table 6, it can be seen that the excited state polarizability estimated by the Abe model is close to that calculated by the HyperChem or DFT method for the ground state of ylids. Nevertheless, a decrease for the excited state dipole moment in the Abe model as

compared to the variational method was obtained. One can hypothesize that the opposite results came from the simplifying hypotheses with which the Abe model works, including the collinearity of the dipole moments of the ground and excited state, and the neglection of the specific interactions between solute and solvent.

3.2. Spectral Study in Ternary Solutions

Recent studies regarding molecular properties estimated by spectral methods have used new theories about the influence of solvent mixtures on solute molecules [50,51]. The advantage of solvent mixtures is that they allow variation of the macroscopic parameters of the solvent in a large range, and one may modify the nature of the intermolecular interactions by choosing suitable solvents. In order to estimate the strength of the possible hydrogen bonds between the hydroxylic solvents and the ylid molecules, spectral studies of a series of ylids were performed and analyzed using a statistical model of the ternary solutions [19,20]. This model was based on the probabilistic expression of occupation of the first solvation sphere of the spectrally active molecule as a function on the composition of the bulk solution. The spectral shift of the absorption band is the contribution of all solvation shells formed around the solute (spectrally active) molecule. The number of solvation shells is proportional to the molar concentration of the solute (around 10^{-3}–10^{-5} mol/L), and each shell has its own composition of the two types of solvent molecules, due to the thermal motion at room temperature. Expression (9) gives the cell model of ternary solutions:

$$\ln \frac{p_1}{1-p_1} = \ln \frac{x_1}{1-x_1} + \frac{w_2 - w_1}{kT} \quad (9)$$

where p and x are the average statistic weight of the active solvent (1) in the first solvation shell of the solute molecule and the molar concentration of the same solvent in the bulk solution; w is the interaction energy between the two molecules, of the solute and the active solvent (1), and of the second solvent (2), which is inactive or barely active from an interaction point of view; k is the Boltzmann constant and T is the absolute temperature.

The average statistic weight of the active solvent (1) in the first solvation shell of the solute, p_1, was determined by using the expression:

$$\nu_t = p_1\nu_1 + (1-p_1)\nu_2 \quad (10)$$

where ν is the wavenumber of the maximum of the absorption band in ternary solution (indexed by t), and in the two solvents, indexed by 1 and 2, respectively.

If the cell statistic model is applicable to spectral data in ternary solutions, one can estimate the difference in the energies of molecular pairs of the following types: solute molecule–solvent (1) molecule, and solute molecule–solvent (2) molecule. This energy is hard, if not impossible, to estimate by common methods. Therefore, application of this particular method becomes very important.

In our study, two ternary solutions of PPPyNiP and PyNiP were prepared using two polar solvents: a protic one (methanol, MeOH) and an aprotic one (N,N′-dimethylformamide, DMF, and dimethylsulfoxide, DMSO). DMF and DMSO have α = 0 and they do not participate in specific interactions by donating protons to ylids, but they have very close values for the β parameter (β = 0.69 for DMF and 0.76 for DMSO, Table 1). MeOH has α = 0.86 and is a highly interacting solvent. In this paradigm, for the difference w_1–w_2, the hydrogen bonding between MeOH and ylids makes a great contribution. The dielectric permittivity measured in our experiments for the mixtures between one protic and one aprotic solvent indicated an increase in the wavenumber of the maximum of the ICT band with the solvent polarity.

In the second analysis, two solvent pairs were used, with both components participating in intermolecular hydrogen bonding: water (1) + methanol (2), and water (1) + ethanol (2). The experimental data obtained for the first two pairs of solvents are listed

in Tables S2–S5. Figure 3 presents graphical representations of $ln\frac{p_1}{1-p_1}$ vs. $ln\frac{x_1}{1-x_1}$ for PP-PyNiP (a) and PyNiP (b).

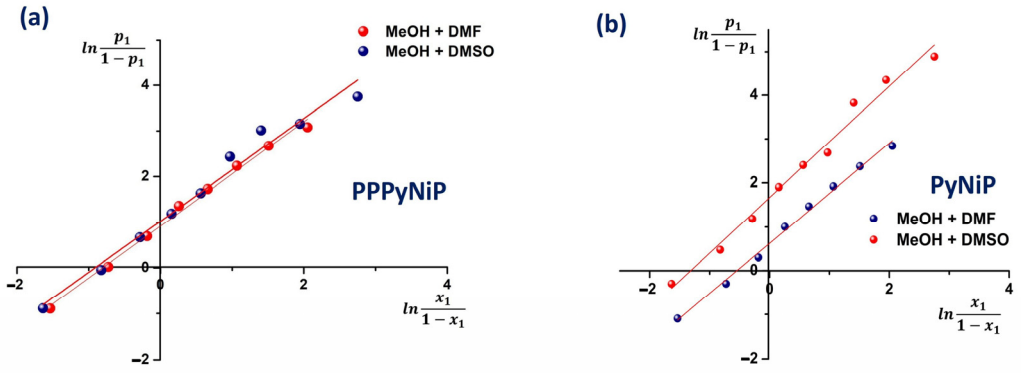

Figure 3. Graphical representation of $ln\frac{p_1}{1-p_1}$ vs. $ln\frac{x_1}{1-x_1}$ for the binary solvents MeOH (1) + DMF (2) and MeOH (1) + DMSO (2) for: (**a**) PPPyNiP; (**b**) PyNiP.

For the binary mixture of hydroxylic solvents MeOH and EtOH, the experimental data are listed in Tables S6–S9. The solvent parameters included in these tables were measured by Buhvestov et al. [52,53]. These parameters indicate an increase in the wavenumber of the maximum of the ICT band with the α parameter (for specific interactions in which the ylid molecules act as proton acceptor) and with π* (for universal interactions). The linear dependences $ln\frac{p_1}{1-p_1}$ vs. $ln\frac{x_1}{1-x_1}$ for the mixtures of hxydroxylic solvents are presented in Figure 4, and the results of the linear regression are listed in Table 7.

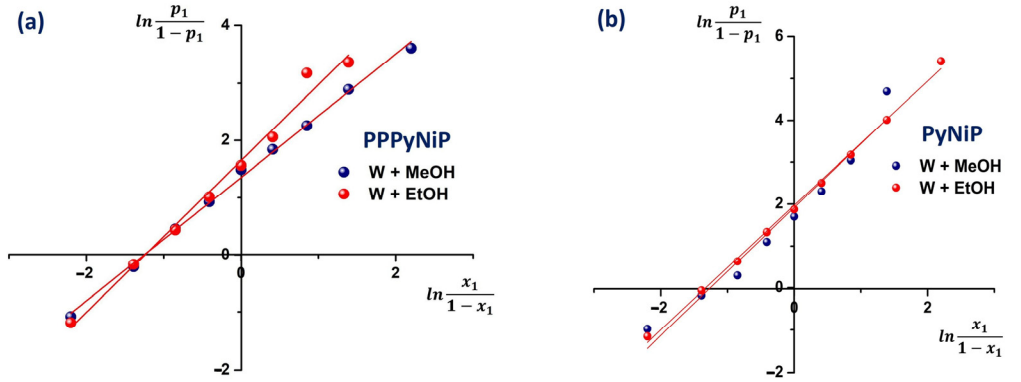

Figure 4. Graphical representation of $ln\frac{p_1}{1-p_1}$ vs. $ln\frac{x_1}{1-x_1}$ for the binary solvents water (W) (1) + MeOH (2) and W (1) + EtOH (2) for (**a**) PPPyNiP and (**b**) PyNiP.

Let us stress out that DMF and DMSO are aprotic solvents, with α = 0, while the values of β are close to that of MeOH, which is a strongly interacting solvent. The influence of proton changes in which the solvent accepts a proton from the solute is almost zero in the w_2–w_1 difference. As such, in the w_2–w_1 expression, the main role is played by the hydrogen bonds established between methanol and the ylid molecules. The value of the w_2–w_1 difference was ≅0.36 kcal/mol for both ylids studied, and such a small value suggests the formation of a very weak hydrogen bond with methanol. Taking into account that the hydrogen bonds stabilize the intermolecular complex, being of negative energies, this results in the hydrogen bonds between water and methylid molecules being about 0.917 kcal/mol for PPPyNiP and about 1.133 kcal/mol for PyNiP. One can consider that the hydrogen bonds between alcohols or water and pyridazinium molecules under study were weak, so they could be destroyed by collisions due to the thermal motion.

Table 7. Values of the slope and intercept determined by linear regression for the $ln\frac{p_1}{1-p_1}$ vs. $ln\frac{x_1}{1-x_1}$ dependences.

Ylid	Solution	Slope	Intercept	R^2	$\omega_2 - \omega_1$ (cal/mol)
PPPyNiP	MeOH + DMF	1.14 ± 0.04	0.92 ± 0.03	0.994	371.70 ± 12.13
	MeOH + DMSO	1.27 ± 0.06	1.67 ± 0.08	0.983	675.45 ± 32.36
	W + MeOH	1.08 ± 0.02	1.35 ±0.02	0.997	546.02 ± 8.09
	W + EtOH	1.32 ± 0.06	1.64 ± 0.07	0.985	663.32 ± 28.31
PyNiP	MeOH + DMF	1.14 ± 0.03	0.62 ± 0.03	0.993	361.28± 12.13
	MeOH + DMSO	1.12 ± 0.06	1.02 ±0.09	0.992	412.55 ± 36.40
	W + MeOH	1.52 ± 0.03	1.91 ± 0.14	0.995	772.52 ± 56.62
	W + EtOH	1.48 ± 0.02	1.96 ± 0.03	0.985	792.74 ± 12.13

3.3. Quantum Chemical Calculations for PPPyNiP and PyNiP

We applied the density functional theory (DFT) and its time-dependent version TD-DFT to analyze the electronic properties of PPPyNiP and PyNiP. We calculated the conformational energy, dipole moment, and polarizability in three solvents with a key influence: cyclohexane (non-polar and non-interacting), methanol (very polar and strongly interacting), and dimethylsulfoxide (very polar and weakly interacting). The optimized geometry of PyNiP and PPPyNiP in vacuo is illustrated in Figure 1. The molecular electrostatic potential obtained at the ω-B97X-D/STO-3G/def2SV level is presented in Figure 5. The red regions, concentrated on the oxygen atoms in the nitro and carbonyl functionalities, correspond to the negative electrostatic potential that is related to the nucleophilic activity. The blue regions are "electrophile", with a positive electrostatic potential and are localized on the hydrogen atoms, covering the whole molecule. It is observed that the length of the *p*-substitution tail in PPPyNiP does not have any influence on the electrostatic potential distribution in the pyridazinium ring.

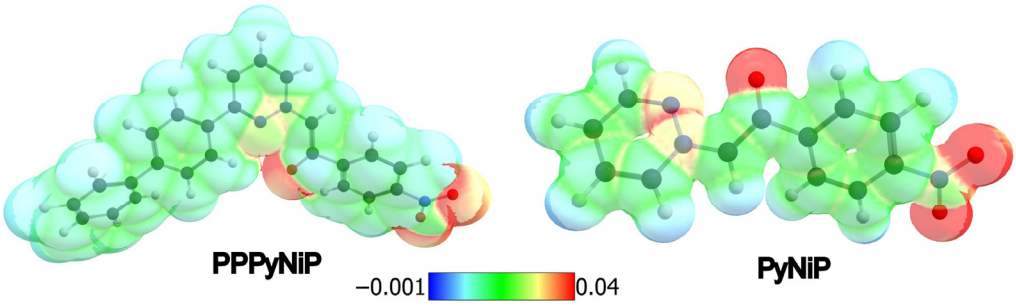

Figure 5. The molecular electrostatic potential of PPPyNiP and PyNiP (isosurface value = 0.002).

Table 8 lists some relevant electronic properties of PPPyNiP and PyNiP, determined by DFT calculations.

It can be observed from Table 7 that the values of the dipole moment grew from the gas state to dimethylsulfoxide, from which we can generalize that this increase is valid from non-polar to polar solvents. The dipole moment in excited state was higher than in the ground state, which confirms the results from the variational model. Judging from the values of ΔE, which is the energy difference in the respective solvent from the vacuo, each molecule was stabilized in solvents with a protic character, such as MeOH, but became less stable in aprotic and highly polar solvents, such as DMSO. This suggests that, for this type of zwitterionic compound, the intermolecular complexes of solute–solvent established by means of hydrogen bonding are more stable than complexes based on electrostatic interactions. In the latter case, this may be due to the re-distribution of the electronic cloud across the ylid molecule that is induced by the high polarizability of the solvent.

Table 8. Calculated values of the dipole moment in the ground and in the excited states, μ_g and μ_e, the energy difference from the vacuo in the ground state (ΔE), the molecular polarizability <α>, and the HOMO—LUMO gap $\Delta E_{H\text{-}L}$, of PPPyNiP and PyNiP.

Ylid	Solvent	μ_g, D	ΔE, eV	<α>, $\times 10^{-24}$ esu	μ_e, D	$\Delta E_{H\text{-}L}$, eV
PPPyNiP	Vacuo	9.40	0	30.143	10.21	6.33
	CHX	10.76	−0.115	32.564	19.41	6.48
	MeOH	11.75	−0.181	36.190	17.11	6.34
	DMSO	11.88	−0.005	36.286	17.24	6.35
PyNiP	Vacuo	7.63	0	18.496	10.21	6.38
	CHX	8.65	−0.095	20.243	12.46	6.23
	MeOH	10.39	−0.144	22.829	13.78	7.18
	DMSO	10.43	0.164	22.897	17.24	7.18

The calculations revealed that the ICT band originates in a HOMO → LUMO transition. The charge transfer direction was obtained by visualizing the frontier molecular orbitals, HOMO and LUMO, pictured in Figure 6 in the energy diagram. One can observe that, whatever the solvent type (apolar, polar aprotic, or protic), the electron density of HOMO was distributed on the heterocycle. Increasing the polarity of the solvent slightly raised the energy of the HOMO level for PPPyNiP, but heavily decreased that of PyNiP. The HOMO-LUMO gaps were around 6.3–6.5 eV for PPPyNiP and became around 7 eV for PyNiP in the very polar solvents. We suppose that this difference in the values of the HOMO-LUMO gap resulted from the electron withdrawing effect of the *p*′-phenyl-*p*-phenyl fragment in PPPyNiP, which seemed to stabilize the electronic density in the molecule. This fragment was also responsible for the higher HOMO level in PPPyNiP as compared to PyNiP.

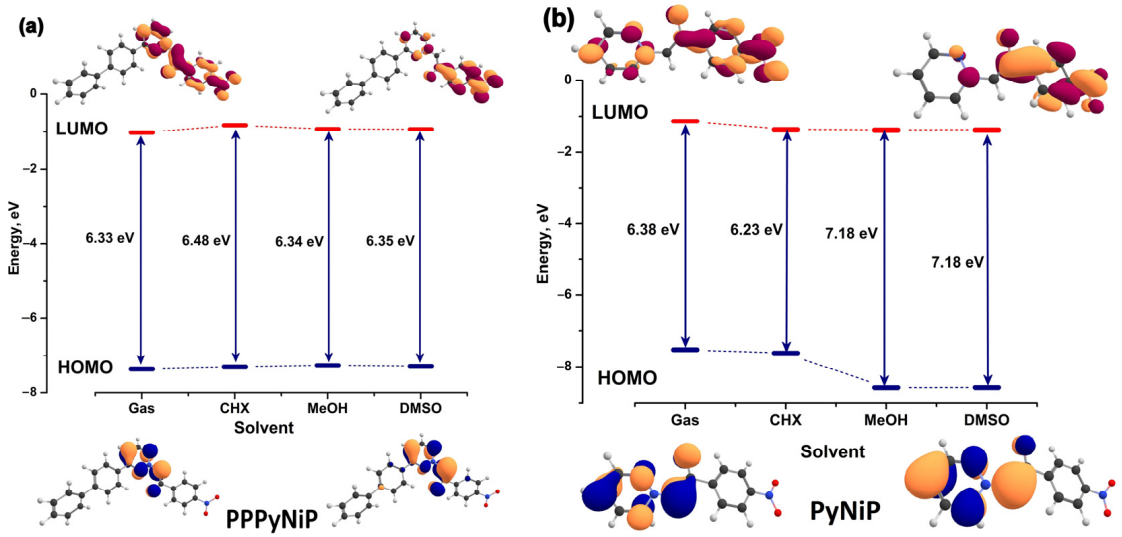

Figure 6. Energy diagram of the predicted frontier molecular orbitals of PPPyNiP (**a**) and PyNiP (**b**) and distribution of the electron density calculated for vacuo and three representative types of solvents: cyclohexane (CHX), methanol (MeOH), and dimethylsulfoxide (DMSO). Yellow regions correspond to the positive orbital phase, and the blue and red regions correspond to the negative orbital phase, respectively. Level of theory: DFT-ω-B97X-D/STO-3G/def2SV/IEF-PCM.

LUMO is mainly localized on the *p*-nitro-phenyl fragment, because the nitro functionality is a strong electron withdrawn substituent. LUMO is gradually restrained and shifted to the *p*-nitro-phenyl fragment as the polarity of the solvent increases, which indicates that the carbanion and the terminal group become a stronger electron acceptor in polar and in interacting solvents. The HOMO–LUMO gap increases with the polarity of the solvent, which rationalizes the negative solvatochromism of both ylids.

Next, the natural transition orbitals, the so-called hole and particle, were calculated, with the purpose of visualizing the change in the electronic density during the ICT transition and comparing them to the canonical orbitals in Figure 6. The HONTO and LUNTO orbitals associated with the ICT transition of PPPyNiP and PyNiP calculated in cyclohexane and dimethylsulfoxide are illustrated in Figures 7 and 8. Similarly, with HOMO and LUMO, the hole had the same localization on the pyridazinium ring, which confirms the prediction from the canonical orbitals. In comparison with LUNTO in Figure 6b, the particle of PyNiP in cyclohexane is spread over almost the whole molecule, which implies that the character of the charge transfer is lowered in the excited state. The increased polarity of DMSO mainly led to the localization of LUNTO of PPPyNiP and PyNiP on the carbanion. In addition, the NTO analysis presented a transition that was, apparently, of a mixed charge transfer/local excited character. The calculated charge displacement was localized on the carbanion in polar solvents and extended to the pyridazinium–*p*-nitro-phenyl fragment in less polar solvents.

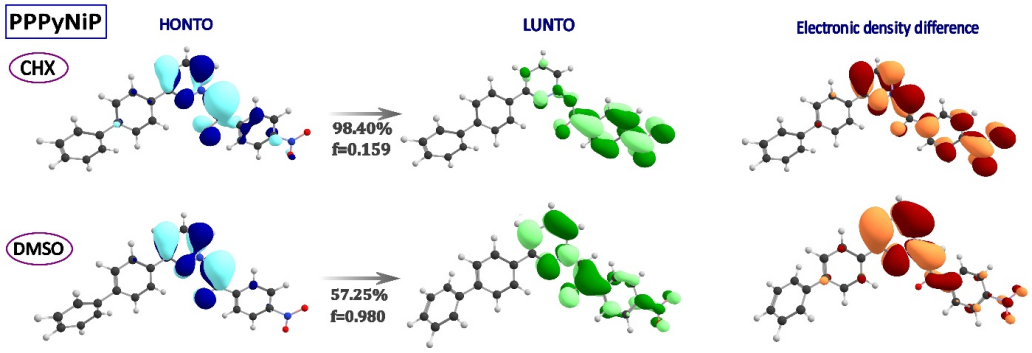

Figure 7. The natural transition orbitals, HONTO and LUNTO, for the ICT transition of PPPyNiP, and the corresponding electronic density difference.

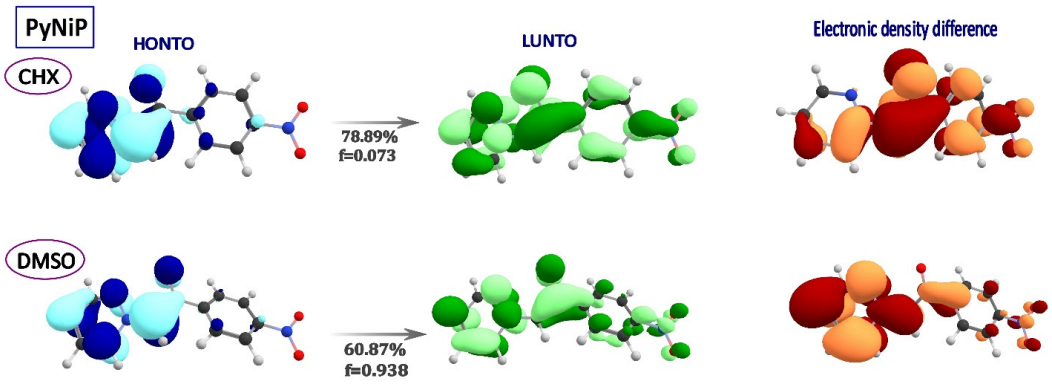

Figure 8. The natural transition orbitals, HONTO and LUNTO, for the ICT transition of PyNiP, and the electronic density difference.

3.4. Pattern Sensitivity to the Type of Solvents

The solvatochromic analysis of PPPyNiP and PyNiP presented in Section 3.1 and the visualization of the molecular orbitals in several kinds of solvents showed that the extent of the charge transfer depends on the type of the solvent. The polarizability of the solvent and the degree of interaction between the solute and the solvent are the key elements that determine the charge transfer process. Therefore, the process of charge transfer in PPPyNiP and PyNiP molecules can be exploited for the development of chemiresistive sensors for the detection of harmful solvents and gases, and for the recognition and separation of dyes and additives with strong coordinating abilities.

As a proof of concept, PPPyNiP and PyNiP were chosen as sensing molecules, and the solvents used in the solvatochromic analysis above were selected as a target. There has been a recent trend in using charged compounds as sensors for solvent discrimination, with the analysis of large datasets, employing statistical analyses [54]. We explored the potential of PPPyNiP and PyNiP for identification of solvents based on the sensitivity of the ICT band. The discriminatory power of the ylids was determined and comparatively evaluated by statistical analysis with the help of principal component analysis (PCA) and cluster analysis (CA). In this regard, a response matrix was constructed from the maximum of the ICT band in the used solvents, using the solvatochromic parameters of the solvents, namely $f(\varepsilon)$, $f(n)$ α, β, and π^*, and two replicates.

The initial number of principal components (PCs) was five, from which only the first two were retained, according to the Kaiser's criterion [55]. The corresponding scree plot is presented in Figure S1. Figure 9 shows how PPPyNiP and PyNiP could distinguish different classes of solvents out of the 24 tested, represented in the canonical plot.

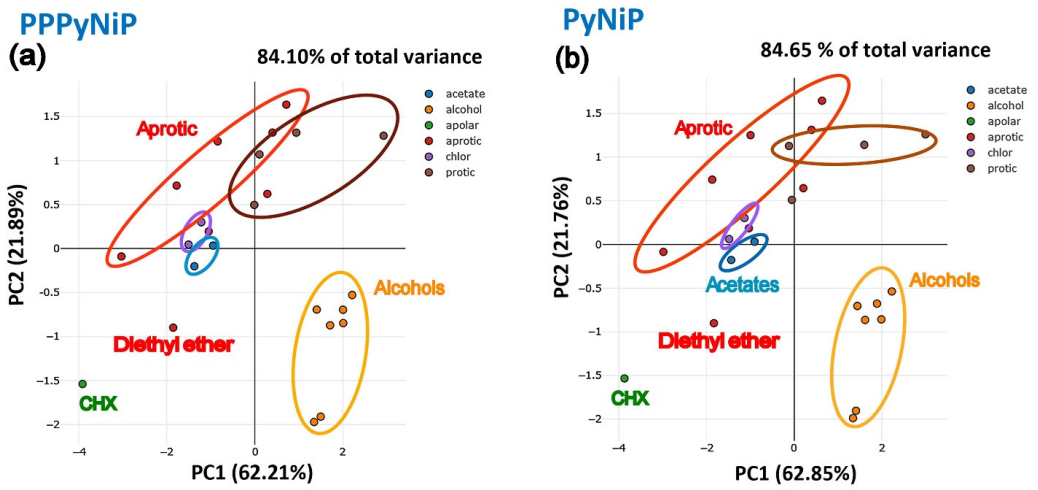

Figure 9. PCA score plots for the response of PPPyNiP (**a**) and PyNiP (**b**) to twenty-four solvents. The first two factors were used, which describe around 85% of the total variance.

The PCA representations of PPPyNiP and PyNiP have the same pattern in terms of the number of PCs and of the spatial separation of groups. The first PC is defined in the direction of the maximum variation of the dataset, and the remaining PCs are orthogonal to each other and define the remaining variance. The first two principal components out of five cover approx. 85% of the total variance, so they reveal a large amount of information about the structure of the groups. PC1 carries 62% of the total weight, and PC2 is about 22%. We infer from this fact that the pyridazinium ring was solely responsible for generating the solvatochromic response, and the influence of the *p*-substituents was negligible. From the clustered data in the first two quadrants, we can make a distinction between aprotic solvents (red color) and acetone and acetophenone (brown color). The large distance between the centroids of alcohols (orange points) and the other groups is indicative of the strong solvatochromic response induced by alcohols, which combine H-bonding abilities (donor and acceptor) with polarizability. Cyclohexane has its own place, from which we conclude that pyridazinium-based compounds can easily recognize inert molecules. Acetates (dark cyan color) and chlorine solvents (purple color) induced a similar solvatochromic reaction and lie near the zero line.

In the next step, a non-hierarchical *Louvain* cluster analysis was applied on the PCA data. The clustering results are presented in Figure 10 for PPPyNiP and in Figure 11 for PyNiP, as a function of the main contributors to the behavior of the ICT band, which were the solvent parameters β, $f(\varepsilon)$, and π^*. We can observe that the datasets contain four clusters for PPPyNiP and three clusters for PyNiP. Nevertheless, the fourth cluster of PPPyNiP contains formamide only, which hints at a distinctive solvatochromic effect that differs

from that in PyNiP. This kind of solvent segregation marks a difference from PCA, where the classification pattern was almost identical for both ylids.

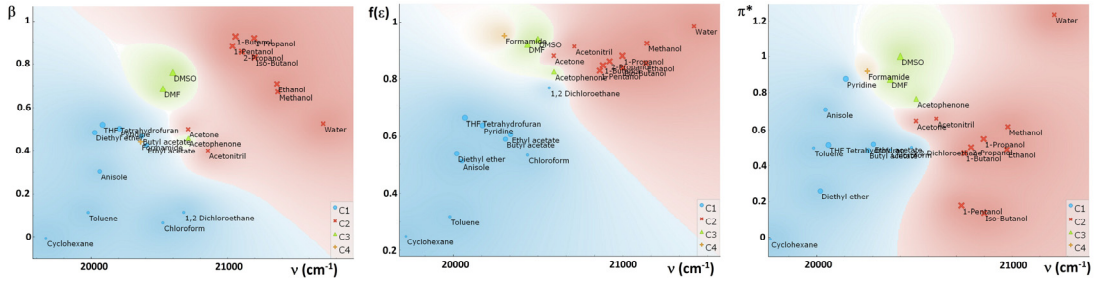

Figure 10. 2D *Louvain* clustering results for PPPyNiP in the principal component space.

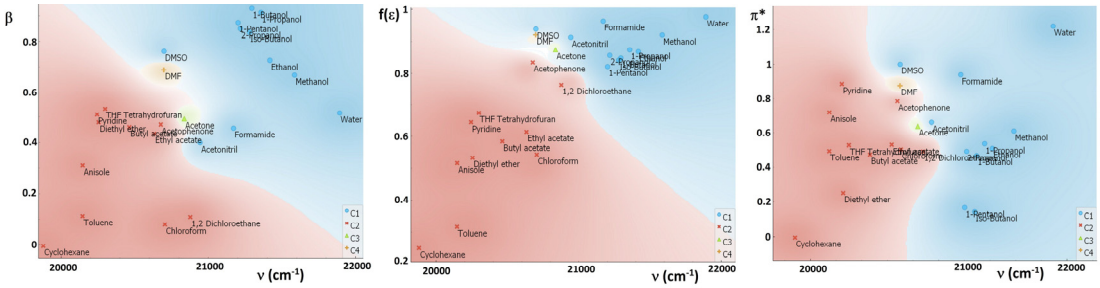

Figure 11. 2D *Louvain* clustering results for PyNiP in the principal component space.

The members of the C1 cluster are the apolar and aprotic solvents, but with acetophenone and acetates staying close to acetone and acetonitrile, which are members of the C2 group. Dimethylsulfoxide and dimethylformamide formed a very distinctive cluster, regardless the solvent parameters used for analysis, for both PPPyNiP and PyNiP. We can explain this segregation by the very close values of $f(\varepsilon)$, $f(n)$ α, β, and π^*. However, the cluster analysis grouped alcohols, acetonitrile, acetone, and formamide together, which does not make sense. In relation to the β parameter of the solvent, however, the plots show a large distance between the alcohol group and the other solvents in the same cluster. Water and cyclohexane are potential outliers, but they were not distinctive enough to be individually clustered.

We can conclude that a more accurate cluster analysis based on solvatochromic behavior requires a larger number of solvents, so that the average sensitivity of the clustering algorithm would increase.

4. Conclusions

A comprehensive solvatochromic study combined with quantum chemical calculation was performed on two carbanion mono-substituted *p*-nitro-phenacyl pyridazinium ylids, focused on the charge transfer band in their absorption spectra. The analysis revealed that the direction of the charge transfer occurred from the heterocycle to the carbanion, which is in opposition to that reported for other cycloimmonium ylids. In the case of the *p*-nitro-phenacyl pyridazinium ylids, the aprotic solvents produced spectral shifts to the red of the visible band, but the specific interactions with the protic solvents determined a redshift of the same band. The negative solvatochromism was confirmed by DFT calculations.

The specific interactions through hydrogen bonding between the OH group of the solvent and the ylid carbanion were weak, and their energy was of about several kcal/mol for the *p*-nitro-phenacyl pyridazinium ylids. Taking into account the energy of the thermal motion at room temperature, at which the absorption spectra were recorded, and the results regarding the strength of the hydrogen bonds of ylids and alcohols, one can see that the thermal motion can destroy the intermolecular complexes realized by H-bonds. As a

result, the composition of the solvation shells in a ternary solution of ylids and alcohols is continuously modified by collision.

Finally, the prospective application of the two studied ylids for the recognition and discrimination of solvents was explored by statistical analysis.

Supplementary Materials: The following supporting information can be downloaded at https://www.mdpi.com/article/10.3390/sym16111531/s1, Figure S1: Scree plot of the PC eigenvalues and the cumulative variance for PPPyNiP and PyNiP. Tables S1–S9. Spectral data in ternary solvents (docx).

Author Contributions: Conceptualization, validation, formal analysis, writing—original draft preparation, writing—review and editing, visualization, supervision: D.O.D. and M.I.A.; methodology, D.O.D. and A.G.-T.; software, M.I.A.; investigation, D.O.D. and A.G.-T.; resources, D.O.D.; data curation, D.O.D. and A.G.-T.; project administration, D.O.D. All authors have read and agreed to the published version of the manuscript.

Funding: This research received no external funding.

Data Availability Statement: Data are contained within the article and Supplementary Materials.

Acknowledgments: No financial support received for this project.

Conflicts of Interest: The authors declare no conflicts of interest.

References

1. Zugravescu, I.; Petrovanu, M. *N-Ylid Chemistry*; McGraw Hill: New York, NY, USA; Acad. Press: London, UK, 1976.
2. Pawda, A. *1,3-Dipolar Cycloaddition Chemistry*; Wiley Interscience: New York, NY, USA, 1984.
3. Butnariu, R.M.; Mangalagiu, I. New pyridazine derivatives: Synthesis, chemistry and biological activity. *Bioorg. Med. Chem.* **2009**, *17*, 2823–2829. [CrossRef] [PubMed]
4. Melnig, V.; Humelnicu, I.; Dorohoi, D.O. Thermal dimerization kinetics of 3-(p-bromo)-pyridazinium benzoyl methylid in solutions. *Int. J. Chem. Kinet.* **2008**, *40*, 230–239. [CrossRef]
5. Ungureanu, M.; Mangalagiu, I.; Petrovanu, M. Pyridazinium ylures in Pharmacy I. *Ann. Pharm. Fr.* **1997**, *55*, 69–77.
6. Mangalagiu, I.; Mangalagiu, G.; Roman, M.; Caprosu, M.; Petrovanu, M. Pyridazinium ylures in Pharmacy II. *Ann. Pharm. Fr.* **2000**, *58*, 86–92.
7. Saxena, H.O.; Faridi, U.; Kumar, J.K.; Luqman, S.; Darokar, M.P.; Shanker, K.; Chanotiya, C.S.; Gupta, M.M.; Negi, A.S. Synthesis of chalcone derivatives on steroidal framework and their anticancer activities. *Steroids* **2007**, *72*, 892–900. [CrossRef]
8. Wu, J.; Batist, C.; Zamfir, L. Identification of a novel steroid derivative, NSC12983, as a paclitaxel-like tubulin assembly promoter by 3-D virtual screening. *Anticancer Drug Des.* **2001**, *16*, 129–133.
9. Popovici, L.; Amarandi, R.M.; Mangalagiu, I.I.; Mangalagiu, V.; Damac, R. Synthesis molecular modelling and anticancer evaluation of new pirrollo[1,2-b]pyridazine and pirrollo[1,2-a]phthalazine derivatives. *J. Enzym. Inhib. Med. Chem.* **2019**, *34*, 230–243. [CrossRef]
10. Mantu, D.; Luca, M.C.; Moldovean, C.; Zvancioc, G.; Mangalagiu, I. Synthesis and antituberculosis activity of some new pyridazine derivatives, Part II. *Eur. J. Med. Chem.* **2010**, *45*, 5164–5168. [CrossRef] [PubMed]
11. Mangalagiu, V.; Damac, R.; Diaconu, D.; Zbancioc, G.; Mangalagiu, I.I. Hybrids diazines; Recent Advancements in Modern Antimicrobial therapy. *Curr. Med. Chem.* **2024**, *31*, 2687–2705. [CrossRef]
12. Ivan, L.M.; Dimitriu, D.G.; Gritco-Todirascu, A.; Morosanu, A.C.; Dorohoi, D.O.; Cheptea, C. Excited state dipole moment of two pyridazinium p-nitro-phenacylids estimated from solvatochromic study. *Spectrosc. Lett.* **2020**, *53*, 1–11. [CrossRef]
13. Dorohoi, D.O. Electronic spectroscopy of N-Ylids. *J. Mol. Struct.* **2004**, *704*, 31–43. [CrossRef]
14. Pop, V.; Dorohoi, D.O.; Holban, V. Molecular interactions in binary solutions of 4-amino-phthalimide and3-p-cumyl-pyridazinium-acetyl-benzoyl-methylid. *Spectrochim. Acta A* **1994**, *50*, 2281–2289. [CrossRef]
15. Dorohoi, D.O.; Holban, V. Intermolecular interactions in some pyridazinium ylids solutions. *J. Mol. Struct.* **1993**, *293*, 133–136. [CrossRef]
16. Homocianu, M.; Airinei, A.; Dorohoi, D.O.; Olariu, I.; Fifere, N. Solvatochromic effects in the UV/Vis absorption spectra of some pyridazinium ylids. *Spectrochim. Acta A* **2011**, *82*, 355–359. [CrossRef]
17. Dorohoi, D.O. Excited state parameters determined by spectral means. *Ukr. J. Phys.* **2018**, *63*, 701–708. [CrossRef]
18. Abe, T. The dipole moments and polarizabilities in the excited state of four benzene derivatives from spectral solvent shifts. *Bull. Chem. Soc. Jpn.* **1967**, *40*, 1571–1574. [CrossRef]
19. Puică-Melniciuc, N.; Avadanei, M.; Caprosu, M.; Dorohoi, D.O. Interaction energy in pairs of phthalazinium dibenzoyl methylid (PDBM)—Protic solvent molecule, estimated in the limits of the cell ternary solution model, by spectral means. *Spectrochim. Acta A* **2012**, *96*, 271–277.

20. Avadanei, M.; Dorohoi, D.O.; Puica Melniciuc, N. Ordering tendency in ternary solutions of pyridazinium ylids evidenced by electron spectroscopy. In Proceedings of the International Conference on Applications of Optics and Photonics, Braga, Portugal, 3–7 May 2011; Proceedings SPIE nr. 3001, art 80012D.
21. Vogel, A. *Textbook of Practical Organic Chemistry*, 4th ed.; Longman: London, UK, 1978; pp. 266–268.
22. Haynes, W.M. (Ed.) *CRC Handbook of Chemistry and Physics*, 95th ed.; CRC Press: Boca Raton, FL, USA; Taylor and Francis: Abingdon, UK, 2014.
23. Lide, D.R. *Handbook of Chemistry and Physics*, 76th ed.; CRC Press: Boca Raton, FL, USA, 1995.
24. Kamlet, M.J.; Abboud, J.I.; Abraham, M.; Taft, R.W. Linear solvation energy relationships 23. A comprehensive collection of the solvatochromic parameters π*, α, β and some methods for simplifying the generalized solvatochromic equation. *J. Org. Chem.* **1983**, *48*, 2877–2887. [CrossRef]
25. Kamlet, M.J.; Abboud, J.I.; Taft, R.W. The solvatochromic comparison method 6. The π* scale of solvent polarities. *J. Am. Chem. Soc.* **1977**, *99*, 6027–6038. [CrossRef]
26. Jessop, P.G.; Jessop, D.A.; Fu, D.; Phan, L. Solvatochromic parameters for solvents of interest in green chemistry. *Green Chem.* **2012**, *14*, 1245–1259. [CrossRef]
27. Reichardt, C. *Solvents and Solvents Effects in Organic Chemistry*, 3rd ed.; Wiley VCH: Weinheim, Germany, 2003.
28. Frisch, M.J.; Trucks, G.W.; Schlegel, H.B.; Scuseria, G.E.; Robb, M.A.; Cheeseman, J.R.; Scalmani, G.; Barone, V.; Mennucci, B.; Petersson, G.A.; et al. *Gaussian 09, Revision A.02*; Gaussian, Inc.: Wallingford, CT, USA, 2009.
29. Pant, D.; Sitha, S. Roles of bridges on Electronic, linear and nonlinear optical Properties: A computational study on zwitterions with N-methyl pyridinium and p-dicyanomethanide phenylene. *Comput. Theor. Chem.* **2023**, *1229*, 114308. [CrossRef]
30. Dorohoi, D.O.; Partenie, D.H.; Chiran, L.M.; Anton, C. About the electronic absorption spectra (EAS) and electronic diffusive spectra (EDS) of some pyridazinium ylids. *J. Chim. Phys. Phys.-Chim. Biol.* **1994**, *91*, 419–431. [CrossRef]
31. Sıdır, İ.; Sıdır, Y.G. Investigation of the interactions of *E*-4-methoxycinnamic acid with solvents: Solvatochromism, electric dipole moment and pH effect. *J. Mol. Struct.* **2018**, *249*, 1161–1171. [CrossRef]
32. Kamlet, M.J.; Abboud, J.I.; Taft, R.W. An examination of linear solvation energy relationships. *Prog. Phys. Org. Chem.* **1981**, *13*, 485–630.
33. Gulseven-Sidir, Y.; Sidir, I.; Demitray, F. Dipole moment and solvatochromism of benzoic acid liquid crystals: Tuning dipole moment and molecular orbital energies by substituted Au under external field. *J. Mol. Struct.* **2017**, *1137*, 440–452. [CrossRef]
34. McRae, E.G. Theory of solvent effects on molecular electronic spectra. Frequency shifts. *J. Phys Chem.* **1957**, *61*, 562–572. [CrossRef]
35. Kawschi, A. On the estimation of excited-state dipole moments from solvatochromic shifts of absorption and fluorescence spectra. *Z. Naturforsch.* **2002**, *57*, 255–262.
36. Dorohoi, D.O.; Gosav, S.; Morosanu, A.; Dimitriu, D.G.; Apreotesei, G.; Gosav, T. Molecular descriptors-spectral property relations for characterizing molecular interactions in binary and ternary solutions. Excited state dipole moment estimation. *Symmetry* **2023**, *15*, 2075. [CrossRef]
37. Dorohoi, D.O.; Creanga, D.E.; Dimitriu, D.G. Intermolecular Interactions in Binary and Ternary Solutions of a Zwitterionic Compound Studied by Solvatochromism. *Symmetry* **2023**, *15*, 563. [CrossRef]
38. Chamma, A.; Viallet, P. Determination du moment dipolaire d'une molécule dans un état excité singulet: Application à l'indole, au benzimidazole et à l'indazole. *C.R. Acad. Sci. Paris Ser. C* **1970**, *270*, 1901–1904.
39. Kawski, A.; Bojarski, P. Comments on the determination of excited state dipole moment of molecules using the method of solvatochromism. *Spectrochim. Acta A Mol. Biomol. Spectrosc.* **2011**, *82*, 527–528. [CrossRef] [PubMed]
40. Gahlaut, R.; Tewari, N.; Bridhkoti, J.P.; Joshi, N.K.; Joshi, H.C.; Pant, S. Determination of ground and excited states dipole moments of some naphthols using solvatochromic shift method. *J. Mol. Liq.* **2011**, *163*, 141–146. [CrossRef]
41. Zakerhamidi, M.S.; Moghadam, M.; Ghanadzadeh, A.; Hosseini, S. Anisotropic and isotropic solvent effects on the dipole moment and photophysical properties of rhodamine dyes. *J. Lumin.* **2012**, *132*, 931–937. [CrossRef]
42. Patil, S.K.; Wari, M.N.; Yohannan Panicker, C.; Inamdar, S.R. Solvatochromic study of coumarin 545 in alcohols for the determination of ground and excited state dipole moments. *Int. J. Adv. Res.* **2013**, *1*, 616–626.
43. Thipperudrappa, J. Analysis of solvatochromism of a biologically active ketocyanine due using different solvent polarity scales and estimation of dipole moments. *Int. J. Life Sci. Pharma Res.* **2014**, *4*, L-1–L-11.
44. Zakerhamidi, M.S.; Golghasemi Sorkhabi, S.; Shamkhali, A.N. Polar and low polar solvents media effect on dipole moments of some diazo Sudan dyes. *Spectrochim. Acta A* **2014**, *127*, 340–348. [CrossRef] [PubMed]
45. Debnath, D.; Purkayastha, A.; Chowdhury, R.; Misra, T.K. Spectral regression analysis of solvent parameters on azoderivatives of 1,3-dimethyl-5-(arylazo)-6-aminouracil and estimation of change in dipole moment from ground to excited state. *J. Indian Chem. Soc.* **2016**, *93*, 989–998.
46. Kaplan, I.G. *Intermolecular Interactions: Physical Picture, Computational Methods and Model Potentials*; John Wiley & Sons: Chichester, UK, 2006.
47. Israelachvili, J.N. *Intermolecular and Surface Forces*, 3rd ed.; Academic Press: Cambridge, MA, USA; Elsevier: Amsterdam, The Netherlands, 2011.
48. Abe, T.; Amako, Z.; Nishioka, T.; Azumi, H. The Dipole Moments and Polarizabilities in the Excited States of Naphthalene from Spectral Solvent Shifts. *Bull. Chem. Soc. Jpn.* **1966**, *39*, 845–846. [CrossRef]

49. Abe, T. Theoretical treatment of Solvent Effects on the Frequency Shifts of Electronic Spectra of Anions. *Bull. Chem. Soc. Jpn.* **1981**, *54*, 327–334. [CrossRef]
50. Suppan, P. Local polarity of solvent mixtures in the field of electronically excited molecules and exciplexes. *J. Chem. Soc. Faraday Trans.* **1987**, *1*, 495–509. [CrossRef]
51. Papadakis, R. Preferential solvation of highly medium responsive pentacyanoferrate (II) complex in binary solvent mixtures. Understanding the role of dielectric enrichment and the specificity of solute-solvent interactions. *J. Phys. Chem. B* **2016**, *120*, 9422–9433. [CrossRef] [PubMed]
52. Buhvestov, U.; Rived, F.; Ràfols, C.; Bosch, E.; Rosés, M. Solute-solvent and solvent-solvent interactions in binary solvent mixtures. Part 7. Comparison of the enhancement of the water structure in alcohol-water mixtures measured by solvatochromic indicators. *J. Phys. Org. Chem.* **1998**, *11*, 185–192. [CrossRef]
53. Pavel, C.M.; Ambrosi, E.; Dimitriu, D.G.; Dorohoi, D.O. Complex formation and micro-heterogeneity in water-alcohol binary mixtures investigated by solvatochromic study. *Eur. Phys. J. Spec. Top.* **2023**, *232*, 415–425. [CrossRef]
54. Du, J.; Deng, Y.; He, Y. A single 9-mesityl-10-methylacridinium ion as a solvatochromic sensor array for multicolor visual discrimination of solvents. *Analyst* **2019**, *144*, 5420–5424. [CrossRef]
55. Kaiser, H.F. The application of electronic computers to factor analysis. *Educ. Psychol. Meas.* **1960**, *20*, 141–151. [CrossRef]